SAND2021-8020J

Journal of Verification, Validation and Uncertainty Quantification

Developing uncertainty quantification strategies in electromagnetic problems involving highly resonant cavities

Salvatore Campione[1]
Sandia National Laboratories
PO Box 5800 MS-1152, Albuquerque NM 87185 USA
sncampi@sandia.gov

J. Adam Stephens[1]
Sandia National Laboratories
PO Box 5800 MS-1318, Albuquerque NM 87185 USA
jasteph@sandia.gov

Nevin Martin[1]
Sandia National Laboratories
PO Box 5800 MS-0829, Albuquerque NM 87185 USA
nevmart@sandia.gov

Aubrey Eckert
Sandia National Laboratories
PO Box 5800 MS-0828, Albuquerque NM 87185 USA
aceckert@sandia.gov

Larry K. Warne
Sandia National Laboratories
PO Box 5800 MS-1152, Albuquerque NM 87185 USA
lkwarne@sandia.gov

Gabriel Huerta
Sandia National Laboratories
PO Box 5800 MS-0829, Albuquerque NM 87185 USA
jghuert@sandia.gov

Robert A. Pfeiffer
Sandia National Laboratories
PO Box 5800 MS-1152, Albuquerque NM 87185 USA
rapfeif@sandia.gov

[1] These authors contributed equally to this work and are joint first authors.

Adam Jones
Sandia National Laboratories
PO Box 5800 MS-1152, Albuquerque NM 87185 USA
adajone@sandia.gov

ABSTRACT

High-quality factor resonant cavities are challenging structures to model in electromagnetics owing to their large sensitivity to minute parameter changes. Therefore, uncertainty quantification strategies are pivotal to understanding key parameters affecting the cavity response. We discuss here some of these strategies focusing on shielding effectiveness properties of a canonical slotted cylindrical cavity that will be used to develop credibility evidence in support of predictions made using computational simulations for this application.

INTRODUCTION

The computational simulation credibility process involves assembling and documenting evidence that can be used to ascertain and communicate the believability of predictions that are produced from computational simulations. The development of capabilities and methods for gathering credibility evidence is a core portfolio to build during the development of a new computational simulation functionality. The collection of credibility evidence often has a specific use case in mind and maps activities to related requirements for that use case. An important aspect of the computational simulation credibility process is uncertainty quantification (UQ). In this paper, we focus on discussing uncertainty quantification strategies for the electromagnetic (EM) modeling of high-quality factor resonant cavities. In general, these cavities exhibit sharp

resonance peaks [1-8], whose features are largely dependent on the geometrical parameters of the cavity. We will first show this strong dependence for a sample slotted cylindrical cavity in Sec. 2, supporting our analysis of uncertainty quantification presented in this paper.

Electromagnetic modeling of these cavities can, in general, be performed through numerical simulation or analytical formulations. While the former is generally slow and may hinder a full uncertainty quantification analysis where a large number of samples may be required, the latter provides a much faster pathway while still capturing the physical phenomena, enabling quick turnaround for sensitivity analysis and down selection of important parameters, as will be shown in Sec. 3. Finally, an uncertainty quantification analysis for the most important parameters identified in Sec. 3 is presented in Sec. 4. These analyses are pivotal to develop credibility evidence in support of predictions made using computational simulations for highly resonant cavities in electromagnetics.

2. DESCRIPTION OF THE ELECTROMAGNETIC PROBLEM OF INTEREST: HIGH-QUALITY FACTOR RESONANT CAVITIES

Some form of electromagnetic shielding is generally introduced to protect electrical circuits and systems from coupling of an external EM environment. This shielding can at times be a formidable task, and often takes the form of an enclosure, e.g., a metallic cavity, which may resonate at certain frequencies. Because enclosures may not be perfectly sealed, external EM fields can penetrate to their interior regions

via various ports of entry, such as joints and apertures. Given that these ports of entry are, in general, small, the enclosure may exhibit resonances with high-quality factor; under this condition, internal field levels can in some cases be much larger than the incoming field [1-8] and potentially interfere with the electrical circuits operation. Shielding effectiveness (SE) is a common quantity that represents the shielding performance of the enclosure, measured as the ratio of the EM field at a given point **r** in space with and without the cavity shield, or:

$$\mathrm{SE}(\mathbf{r}) = \frac{\left|\mathbf{E}_{\mathrm{cavity}}(\mathbf{r})\right|}{E_0}. \tag{1}$$

In Eq. (1), $\mathbf{E}_{\mathrm{cavity}}(\mathbf{r})$ is the field inside the cavity at location $\mathbf{r}$ and E_0 is the external incident electric field strength. Note this quantity also largely depends on the frequency of the excitation. In general, shielding effectiveness is plotted in units of dB, which is obtained by computing $20\log_{10}(\mathrm{SE})$ in Eq. (1).

An example of enclosure is represented by the structure shown in Fig. 1(a): an aluminum-alloy cylinder with thickness *d* and metal conductivity σ , with interior height *h* and interior radius *a*. These parameters (in addition to the slot) define the resonant frequencies of transverse magnetic (TM) and transverse electric (TE) modes [6, 8-10] supported by the cavity. A port of entry is introduced as an azimuthal slot on one side of the cylinder located midway along the cylinder height, with a width *w* and a length ℓ (in what follows, the projected length used to setup the geometry in the simulation is computed from the formula $\ell = 2a\sin^{-1}\left[\ell_p/(2a)\right]$). Note that the slot acts as a current source drive for the interior cavity modes from the exterior fields at the

frequencies analyzed in this paper below the slot resonance. To probe TM modes, we excite the cavity with an external plane wave source propagating along the –*x*-direction and with electric field polarized along the *z*-direction as shown in Fig. 1(a).

The shielding effectiveness properties of the cavity in Fig. 1(a) are shown in Fig. 1(b) around the resonant frequency of the TM_{010} mode at about 1.129 GHz using the analytical unmatched formulation reported in Appendix B. One can observe very sharp resonance peaks with SE peak values well above 0 dB, signature of very strong fields within the cavity. Furthermore, one can note the strong dependence of SE to the geometrical parameters of the slot: a mere change of 20 mils in slot width caused a change of 8.2 dB in peak SE. This brief analysis shows that small changes in cavity parameters may result in large changes in SE, thus justifying our analysis of uncertainty quantification presented in this paper.

3. SENSITIVITY ANALYSIS OF HIGH-QUALITY FACTOR RESONANT CAVITIES USING DAKOTA

Sensitivity analysis is a tool to identify important inputs and to characterize their relationship with the output [11]. For the use case investigated in this paper, there were two goals of the sensitivity analysis:

1) Reduce the dimensionality of the input space by identifying whether any uncertain inputs have little effect on SE. These inputs can then be held constant in subsequent analyses.
2) Understand which uncertain inputs have the strongest impact on SE, which may then prompt additional studies of those inputs.

An important feature of sensitivity analysis owes to the fact that probability distributions of each parameter are not required to rank parameter sensitivity.

The matched power balance analytical model briefly summarized in Appendix A was used for sensitivity analysis as it is a computationally efficient representation of the full-wave EIGER simulation method, a higher fidelity method of moments code developed at Sandia National Laboratories [12, 13]. For this analysis, six uncertain inputs were considered with ranges specified in Table 1. These ranges are not meant to capture physical uncertainties, but rather to highlight how these parameters affect shielding effectiveness; a proper determination of their uncertainties will be performed in future work.

The sensitivity analysis (and the uncertainty analysis described in Sec. 4) was performed using Dakota [14], a software toolkit developed at Sandia National Laboratories for optimization, sensitivity analysis, and UQ. There are many methods for performing sensitivity analysis [15], but a common approach is to calculate global sensitivity metrics that can be used to quantify the effect of uncertainty in the inputs on the uncertainty in the quantity of interest (QoI). Variance based indices [16] (also known as Sobol indices [17]) were used to decompose the variance in SE and attribute it to one of the uncertain inputs. To calculate the indices, consider the following representation of the power balance model:

$$\mathrm{SE} = f(\mathbf{x}) \tag{2}$$

where $\mathbf{x} = [x_1, \ldots, x_6]$ is a vector of the 6 uncertain input variables and f is the power balance model. The first-order sensitivity index (also called the main effect) of input x_j can be calculated as:

$$S_j = \frac{Var_{x_j}\left(E_{\mathbf{x}_{(-j)}}\left[\mathrm{SE} \mid x_j\right]\right)}{Var\left(\mathrm{SE}\right)} \tag{3}$$

where $E_{\mathbf{x}_{(-j)}}\left[\mathrm{SE} \mid x_j\right]$ is the expected value taken for all variables except x_j of the SE conditional on input x_j, with $j = 1,\ldots,6$, $\mathbf{x}_{(-j)}$ is a vector of all the uncertain inputs except the j^{th} input, and *Var* denotes the variance of the argument. The quantity S_j in Eq. (3) gives a measure of how the conditional expected value varies as the j^{th} input changes after being scaled by the total variation of SE across all inputs. In other words, S_j gives the proportion of the variance of SE that can be attributed to the j^{th} input. This will give a measure of the importance of the j^{th} input alone. However, in many cases, there are interactions between inputs (i.e., the effect of one input on the output changes based on the value of another input). Therefore, an additional metric that is often used is the total-order sensitivity index, defined as:

$$T_j = \frac{E_{\mathbf{x}_{(-j)}}\left\{Var_{x_j}\left(\mathrm{SE} \mid \mathbf{x}_{(-j)}\right)\right\}}{Var\left(\mathrm{SE}\right)} = 1 - \frac{Var_{\mathbf{x}_{(-j)}}\left(E_{x_j}\left[\mathrm{SE} \mid \mathbf{x}_{(-j)}\right]\right)}{Var\left(\mathrm{SE}\right)} \tag{4}$$

The quantity T_j in Eq. (4) gives the proportion of the variance in SE that can be attributed to the j^{th} input, along with its interactions with other inputs. If T_j is much larger than S_j, it indicates that there are significant interactions with the j^{th} input that contribute to the variance in SE. Alternatively, when the difference between these quantities is small, the interactions with the j^{th} input are negligible.

The expectations and variances in Eqs. (3) and (4) are estimated using high dimensional integrals that often require a Monte Carlo (MC) integration approach to solve [11]. The MC approach requires many runs of the model to estimate the integrals, and therefore, a surrogate model (i.e., a computationally efficient approximation) is often used in place of the model. In this case, a polynomial chaos expansion (PCE) model was used as a surrogate to the power balance model to estimate the indices [18]. The PCE approach employs bases of multivariate orthogonal polynomials to capture the functional relationship between a response and input random variables. Once the expansion has been constructed, Eqs. (3) and (4) may be evaluated in closed form, yielding estimates of the variance-based indices. Dakota implements the generalized PCE scheme, in which the particular polynomials used are based on the distributions of the input variables.

In this instance, the PCE models were constructed via regression. Dakota features several compressed sensing techniques for performing regression; here we employed orthogonal matching pursuit. Additional explanation and implementation details have been reported in [19]. A training dataset was created from the results of 448 runs of the matched power balance model (see Appendix A). The 448 points in parameter space were selected using Latin Hypercube sampling. Each run produced a prediction of the shielding effectiveness at 51 equally-spaced frequencies between 1 and 3 GHz, and a separate PCE model was constructed at each frequency. To reduce overfitting, 10-fold cross validation (CV) was used to separately select the order of each expansion. Dakota uses the mean squared error (MSE) for cross validation of PCE

models. Total orders between 1 and 4 were explored, and for all frequencies, 4th order PCEs produced the lowest CV scores, which were all between 3×10^{-4} and 7×10^{-4}.

The resulting variance-based indices over the whole frequency range considered are shown in Fig. 2. There it can be seen that slot width *w* and slot length ℓ were the highest contributors to the uncertainty in the SE across all frequencies, with slot width contributing 70%- 80% of the variation in SE. The cavity parameters (i.e., height *h*, radius *a*, and conductivity σ) and slot depth *d* contributed a negligible amount, though for low frequencies (i.e., less than 1.5 GHz), slot depth contributed slightly more than the other three parameters. The total-order indices T_j shown as dotted lines in Fig. 2 are similar to the first-order indices S_j, especially at lower frequencies, implying that there are likely not significant interactions present. These results were confirmed using the unmatched formulation model in Appendix B at select resonant modes.

While the results in Fig. 2 allow us to rank the parameters affecting SE, to quantify the SE change from each individual parameter in a more direct way, we plot SE versus frequency while varying each input parameter in Fig. 3. In particular, the plots in Fig. 3 were generated by uniformly sampling each input across its range while holding the other inputs constant at their midpoints. The yellow line represents the mean SE, while the black lines represent the minimum and maximum SE. The width between the black lines gives an estimate of the effect of each input on the SE. This plot confirms the results derived from the Sobol indices in Fig. 2, and both plots help build a more robust credibility evidence.

Since the uncertainty in the cavity parameters was found to contribute a negligible amount to the uncertainty in SE across frequency, it was decided to hold the cavity parameters fixed at nominal values. Namely, the cavity height, radius and conductivity were fixed at 24 inch, 4 inch, and 2.6×10^7 S/m, respectively, for the remainder of the analyses. This process showed that the analytical power balance models could be used to down select uncertain input parameters for future analyses.

4. UNCERTAINTY ANALYSIS OF HIGH-QUALITY FACTOR RESONANT CAVITIES USING DAKOTA

Once the dimensionality of the uncertain input space was reduced as shown in Sec. 3, the next step was to characterize the uncertainty in SE. The goals of this second analysis were again twofold:

1. Estimate the range (i.e., minimum and maximum) of SE based on the range of the remaining three uncertain inputs. This is referred to as an interval uncertainty analysis [20].
2. Compare the results of an analytical code to a full-wave, higher fidelity code to assess whether the analytical code could be used for a full probabilistic uncertainty analysis.

It is important to briefly discuss the distinction between an interval and a probabilistic uncertainty analysis. In the former case, uncertain inputs are bounded by minimum and maximum values, and the objective is to estimate the minimum and maximum SE, as shown in the notional example in Fig. 4. The benefits of this type of analysis are that probability distributions do not need to be defined for the uncertain inputs (a nontrivial task) and that in situations where the input/output relationship is simple (e.g., roughly linear, as is the case in our example), a relatively small number of

model runs are required to accurately estimate the range of SE. The primary disadvantage is that statements about the likelihood of different values within that range cannot be made. For example, it would not be possible to estimate the probability that the SE is above, say, 20 dB using this approach. In the latter case, probability distributions must be defined for the uncertain inputs, and these probability distributions are typically sampled in a Monte Carlo procedure and then propagated through the model. The result is a probability distribution on the QoI from which probabilistic statements can be made (see Fig. 5).

The first step was to compare an analytical model against a higher fidelity model for an interval analysis as this can be done with a relatively small number of model runs. We employ here the unmatched formulation reported in Appendix B that provides SE spectra around resonant modes. The results from this analytical model are compared to those of EIGER for the TM_{010} resonant mode.

The interval uncertainty analysis was performed considering slot depth *d*, slot width *w*, and slot length ℓ_p with the minimum and maximum values that are defined in Table 2 (cavity radius, height, and metal conductivity were kept fixed at 4 inch, 24 inch, and 2.6×10^7 S/m respectively). A 4^3 full factorial design [21] was used, where the exponent '3' represents the number of uncertain inputs and the base '4' represents the number of levels for each input. The four levels were chosen to be equally spaced within the range of each input as detailed in Table 2. This resulted in 64 model runs comprising of every combination of the input parameters.

This 4^3 full factorial design was chosen as the relationship between the inputs and outputs was expected to be roughly linear, but it was of interest to confirm this by assessing whether quadratic or cubic effects were present. It also allowed for the estimation of the range of SE with a relatively limited number of model runs. This design was run for both the unmatched formulation in Appendix B and EIGER, and the results are shown in Fig. 6. Immediately obvious is the good agreement between the unmatched formulation and EIGER across the entire input space; this indicates that the unmatched formulation is a good choice for a more computationally expensive probabilistic uncertainty analysis. Additionally, these results are consistent with those seen on the matched bound sensitivity analysis described in Sec. 3. In particular, slot width and length have the most effect on the peak SE, and there do not appear to be significant interactions among different input parameters. This is easily identifiable by the fact that the lines in Fig. 6 are roughly parallel.

Because of the good agreement between the unmatched formulation and EIGER results shown in Fig. 6, we decided that the former could be used for a probabilistic uncertainty analysis. Currently, there is not a strong physical basis for the choice of input distributions for the uncertain inputs. However, it was of interest to exercise Dakota for uncertainty propagation and to understand how different distributional choices might affect the QoI. Therefore, a probabilistic uncertainty analysis was performed under both uniform and normal distributional assumptions, as defined in Table 3. The mean and standard deviation for the normal distributions were derived from the lower and upper bounds of the uniform distributions; the means are the

midpoints, and the standard deviations are 1/6 of the range. This standard deviation was chosen such that approximately 99.7% of the distribution falls within the bounds specified for each input. This choice was somewhat arbitrary - alternatives could be increasing the number of standard deviations within the range or making the variance of the normal distribution equal to that of the uniform. In addition to assessing how different input distributions affect the QoI, we also wished to examine the consequences of reducing the initial set of six input parameters listed in Table 1 to the three most influential ones (the slot dimensions) identified by our sensitivity analysis and listed in Table 2.

To achieve well-converged results, we once again employed PCE surrogates, which can be sampled very inexpensively. Using a procedure similar to the one described in Sec. 3, we created a total of four training sets and models, one for each combination of distribution assumption and variable set (all 6 input parameters versus 3). Dakota was used to perform Latin Hypercube sampling on unmatched formulation model to obtain training data. For the two 6-input cases, the training sets included 112 samples, and for the 3-input cases, 64. (For the 3-input cases, the three parameters that were not varied were fixed at their means/midpoints.) PCE orders up to five were considered; Table 4 lists the selected order and their cross-validation scores.

The PCE models for the four cases considered were sampled 10^5 times, and the resulting histograms of SE are shown in Fig. 7. One can see that the two SE distributions (full sets of parameters versus down selected parameters) are virtually the same

(besides small differences around the right tail of the distributions), confirming that the slot parameters are the most important parameters for SE determination.

The inset of Fig. 7 illustrates some of the consequences of input distribution selection. While the two distributions are centered at similar values of SE, the distribution is noticeably wider in the uniform case. This observation is consistent with the statistics that are reported in Table 5. For example, the standard deviation of SE for the uniform case is more than 75% greater (5.5 dB versus 3.1 dB) than for the normal case. These results show the importance of selecting input distributions appropriately, particularly when low-probability events in the tails of the distributions matter.

CONCLUSIONS

The development of methods and capabilities for use in uncertainty quantification for EM problems is an important aspect of gathering credibility evidence to support predictions derived from computational simulation analyses. The work presented in this paper gives an exemplar for uncertainty quantification and sensitivity analysis in this application space. In particular, we performed a sensitivity analysis for a slotted cylindrical cavity and ranked the contribution to the QoI from each of the input parameters. We observed no interaction among different inputs and determined that the slot parameters are the most important for the evaluation of SE. We then compared the results from the analytical, unmatched bound code to EIGER to assess whether the unmatched bound code could accurately bound the SE. Finally, we performed an uncertainty quantification analysis of SE assuming two distributions for the uncertain

input parameters and observed a strong dependence on the distribution of the QoI from the distribution of the inputs. This exemplar will be used as a prototype for the application of uncertainty and sensitivity analysis methods to more complex electromagnetic computational simulation analyses in the future.

ACKNOWLEDGMENT

We acknowledge Dr. Aaron J. Pung, Sandia National Laboratories, for the construction of Fig. 1(a). This work was partially supported by the Laboratory Directed Research and Development program at Sandia National Laboratories. Sandia National Laboratories is a multimission laboratory managed and operated by National Technology and Engineering Solutions of Sandia, LLC, a wholly owned subsidiary of Honeywell International, Inc., for the U.S. Department of Energy's National Nuclear Security Administration under contract DE-NA-0003525. This paper describes objective technical results and analysis. Any subjective views or opinions that might be expressed in the paper do not necessarily represent the views of the U.S. Department of Energy or the United States Government.

FUNDING

Partially supported by the Laboratory Directed Research and Development (LDRD) program at Sandia National Laboratories.

NOMENCLATURE

UQ	Uncertainty quantification
EM	Electromagnetic
SE	Shielding effectiveness
TM	Transverse magnetic
TE	Transverse electric
r	Location point inside the cavity
$\mathbf{E}_{\text{cavity}}(\mathbf{r})$	Field inside the cavity at location **r**
E_0	External incident electric field strength
d	Cavity thickness and slot depth
h	Interior cavity height
a	Interior cavity radius
w	Slot width
σ	Metal conductivity
ℓ_p	Projected slot length
ℓ	Slot length
S_j	First-order sensitivity index
T_j	Total-order sensitivity index

MC	Monte Carlo
PCE	Polynomial chaos expansion
CV	Cross validation
MSE	Mean squared error
QoI	Quantity of interest
P_{rec}	Received power of the aperture with backing cavity
P_{wall}	Absorption in the cavity walls
A	Interior cavity wall surface area
ω	Angular frequency
μ_0	Absolute permeability of free space
R_S	Surface resistance
$\left\langle \left\| H_j \right\|^2 \right\rangle_A$	Mean squared magnetic field component on the wall
H_0	Incident magnetic field
$SE_{\max}$	Approximate extreme value of the mean shielding effectiveness
E_z	Interior electric field for fundamental TM modes
$A_{m,p,n}$	Coefficient to account for coupling through the slot

REFERENCES

[1] M. P. Robinson, T. M. Benson, C. Christopoulos, J. F. Dawson, M. D. Ganley, A. C. Marvin*, et al.*, "Analytical formulation for the shielding effectiveness of enclosures with apertures," *IEEE Transactions on Electromagnetic Compatibility,* vol. 40, pp. 240-248, 1998.

[2] X.-C. Nie and N. Yuan, "Accurate Modeling of Monopole Antennas in Shielded Enclosures with Apertures," *Progress in Electromagnetics Research,* vol. 79, pp. 251-262, 2008.

[3] S. Eng Swee, K. Sertel, J. L. Volakis, V. V. Liepa, and R. Wiese, "Coupling studies and shielding techniques for electromagnetic penetration through apertures on complex cavities and vehicular platforms," *IEEE Transactions on Electromagnetic Compatibility,* vol. 45, pp. 245-257, 2003.

[4] G. B. Tait, C. Hager, M. B. Slocum, and M. O. Hatfield, "On Measuring Shielding Effectiveness of Sparsely Moded Enclosures in a Reverberation Chamber," *IEEE Transactions on Electromagnetic Compatibility,* vol. 55, pp. 231-240, 2013.

[5] L. K. Warne, R. E. Jorgenson, J. T. Williams, L. I. Basilio, W. L. Langston, R. S. Coats*, et al.*, "A Bound on Electromagnetic Penetration through a Slot Aperture with Backing Cavity," Sandia National Laboratories report SAND2016-9029, Albuquerque, NM, USA,2016.

[6] S. Campione, I. C. Reines, L. K. Warne, J. T. Williams, R. K. Gutierrez, R. S. Coats*, et al.*, "Preliminary Survey on the Effectiveness of an Electromagnetic Dampener to Improve System Shielding Effectiveness," *Sandia National Laboratories Report* SAND2018-10548, Albuquerque, NM, 2018.

[7] S. Campione, I. C. Reines, L. K. Warne, C. Grimms, J. T. Williams, R. K. Gutierrez*, et al.*, "Perturbation theory to model shielding effectiveness of cavities loaded with electromagnetic dampeners," *Electronics Letters,* vol. 55, pp. 644-646, 2019.

[8] S. Campione, L. K. Warne, W. L. Langston, R. A. Pfeiffer, N. Martin, J. T. Williams*, et al.*, "Penetration through slots in cylindrical cavities operating at fundamental cavity modes," *IEEE Transactions on Electromagnetic Compatibility,* vol. 62, pp. 1980-1988, 2020.

[9] S. Campione, L. K. Warne, L. I. Basilio, R. S. Coats, and R. E. Jorgenson, "Antenna Loading Impact on the Coupling Response of a Slotted Cylindrical Cavity," *Sandia National Laboratories Report* SAND2017-5378, Albuquerque, NM, 2017.

[10] R. F. Harrington, *Time-Harmonic Electromagnetic Fields* vol. Chapters 1, 5, 7: Wiley-IEEE Press, 2001.

[11] A. Saltelli, M. Ratto, T. Andres, F. Campolong, J. Carboni, D. Gatelli*, et al.*, *Global Sensitivity Analysis. The Primer.* : John Wiley and Sons, Ltd., 2008.

[12] R. M. Sharpe, J. B. Grant, N. J. Champagne, W. A. Johnson, R. E. Jorgenson, D. R. Wilton*, et al.*, "EIGER: Electromagnetic interactions GEneRalized," *Sandia National Laboratories Report* SAND97-0576C, Albuquerque, NM, 1997.

[13] D. R. Wilton, W. A. Johnson, R. E. Jorgenson, R. M. Sharpe, and J. B. Grant, "EIGER: A new generation of computational electromagnetics tools," *Sandia National Laboratories Report* SAND96-0646C, Albuquerque, NM, 1996.

[14] B. M. Adams, L. E. Bauman, W. J. Bohnhoff, K. R. Dalbey, M. S. Ebeida, J. P. Eddy, *et al.*, "Dakota, A Multilevel Parallel Object-Oriented Framework for Design Optimization, Parameter Estimation, Uncertainty Quantification, and Sensitivity Analysis: Version 6.11 User's Manual," Sandia National Laboratories, Albuquerque, NM, 2019.

[15] J. C. Helton, J. D. Johnson, C. J. Sallaberry, and C. B. Storlie, "Survey of sampling-based methods for uncertainty and sensitivity analysis," *Reliability Engineering and System Safety,* pp. 1175-1209, 2006.

[16] T. Homma and A. Saltelli, "Importance measures in global sensitivity analysis of model output," *Reliability Engineering and System Safety,* pp. 1-17, 1996.

[17] I. M. Sobol, "Theorems and examples on high dimensional model representation," *Reliability Engineering and System Safety,* pp. 187-193, 2003.

[18] B. Sudret, "Global sensitivity analysis using polynomial chaos expansions," *Reliability Engineering and System Safety,* vol. 93, pp. 964-979, 2008.

[19] B. Adams, M. Eldred, G. Geraci, R. Hooper, J. Jakeman, K. Maupin, *et al.*, "Dakota, A Multilevel Parallel Object-Oriented Framework for Design Optimization, Parameter Estimation, Uncertainty Quantification, and Sensitivity Analysis: Version 6.11 Theory Manual," Sandia National Laboratories, Albuquerque, NM, 2019.

[20] M. Eldred, L. Swiler, and G. Tang, "Mixed aleatory-epistemic uncertainty quantification with stochastic expansions and optimzation-based interval estimation," *Reliability Engineering and System Safety,* vol. 96, pp. 1092-1113, 2011.

[21] D. Montgomery, *Deisgn and Analysis of Experiments*: John Wiley & Sons, 2013.

[22] K. S. H. Lee and F.-C. Yang, "Trends and bounds in RF coupling to a wire inside a slotted cavity," *IEEE Transactions on Electromagnetic Compatibility,* vol. 34, pp. 154-160, 1992.

APPENDIX A. ANALYTICAL POWER BALANCE MODEL

We briefly recall here a power balance analytical model reported in [5, 8] that will be used to determine and rank the importance of geometrical and material parameters through a sensitivity analysis. This model was used to define an upper bound, wide-band SE result for a slot aperture by treating the backing cavity as a uniformly distributed matched load [5, 8], requiring large values of cavity conductivity. We implicitly assume a time dependence of the kind $\exp(-i\omega t)$. Below the slot resonance frequency, and for an electrically short slot matched bound case, the shielding effectiveness can be estimated from power results using conservation of power arguments [22], for which:

$$\frac{\ell |H_0|^2 \left(8/\pi^2\right)}{R_{\text{int}}\pi^2/\left(\omega L \ell\right)^2 + G_{rad}} = P_{rec} = P_{wall} = 2AR_S \left\langle \left|H_j\right|^2 \right\rangle_A \tag{5}$$

where P_{rec} is the received power of the aperture with backing cavity, P_{wall} is the absorption in the cavity walls, $A = 2\pi a^2 + 2\pi ah$ is the interior cavity wall surface area of a cylindrical cavity, $R_S = \sqrt{\omega\mu_0/(2\sigma)}$ is the surface resistance, ω is the angular frequency, μ_0 is the absolute permeability of free space, σ is the metal conductivity of the cavity walls, $\left\langle \left|H_j\right|^2 \right\rangle_A$ is the mean squared magnetic field component on the wall, H_0 is the incident magnetic field, $L = \mu_0\pi/\Omega_e$, $\Omega_e = \Omega + C_e$, $\Omega = 2\ln\left(\ell/a_{eq}\right)$, $C_e = 2\left(\ln 2 - 7/3\right)$, $a_{eq} = 2w/\left(\pi \exp^{1+\pi d/(2w)}\right)$. Furthermore, $R_{\text{int}} = \text{Re}\left(Z_{\text{int}}\right)$ with $Z_{\text{int}} = \left(L/L^{\text{int}r}\right)^2 Z_{\text{int}}^{\text{int}r}$,

$Z_{\text{int}}^{\text{int}r} = 2Z_S / d$, $Z_S = (1+i)R_S$, $L^{\text{int}r} = \mu_0 w / d$ and G_{rad} is given by

$$\pi\eta_0 \ell G_{rad} = -\left[1+\cos(k\ell)\right] + \left(\frac{k\ell}{2\pi} + \frac{\pi}{2k\ell}\right)\left[Cin(k\ell+\pi) - Cin(\pi-k\ell)\right] + \frac{k\ell}{2}\left[1-\left(\frac{\pi}{k\ell}\right)^2\right]\left[Si(k\ell+\pi) - Si(\pi-k\ell)\right],$$

where the standard cosine and sine integrals are $Cin(z) = \int_0^z \{1-\cos(u)\}\frac{du}{u} = -Ci(z) + \ln z + \gamma'$ and $Si(z) = \int_0^z \sin(u)\frac{du}{u}$, and γ' is the Euler's constant. Using Eq. (5), we can compute $\left\langle |H_j|^2 \right\rangle_A = P_{rec} / (2AR_S)$, which we can then use to calculate the approximate extreme value (using the peak to average ratio for a two or three dimensional standing wave) of the mean shielding effectiveness as:

$$SE_{\max} \approx 4\langle SE \rangle = 4\frac{\left\langle |H_j|^2 \right\rangle_A}{|H_0|^2}. \tag{6}$$

APPENDIX B. ANALYTICAL UNMATCHED FORMULATION MODEL

We briefly recall here an unmatched formulation analytical model reported in [8] that, as opposed to the matched power bound model reported in Appendix A, provides an actual level of shielding effectiveness around individual resonant modes. We implicitly assume a time dependence of the kind $\exp(-i\omega t)$. For fully-enclosed cylindrical cavities with internal height *h* and internal radius *a*, the *z*-component of the interior electric field for fundamental TM modes with E_z even in *z* and *φ* with indices (m,p,n) in space for $0 < \phi < 2\pi$, $0 < \rho < a$, $-h/2 < z < h/2$ is

$$E_z = A_{m,p,n} J_m\left(\varsigma_{m,p}\rho\right)\cos\left(m\phi\right)\cos\left(\alpha_n z\right) \tag{7}$$

with $\varsigma_{m,p} = j_{m,p}/a$, $\alpha_n = n\pi/h$, $J_m\left(\rho\right)$ the Bessel function of first kind of order *m*, $j_{m,p}$ zeroes of $J_m\left(\rho\right)$, $p = 1,2,\ldots$, and $n = 0,1,2,\ldots$. The coefficients $A_{m,p,n}$ account for the coupling through the slot and are given by

$$A_{m,p,n} = -\frac{4\varepsilon_n\varepsilon_m}{3\pi hb}\frac{\ell}{2}\frac{V\left(0\right)\cos\left(m\phi_{\mathrm{s}}\right)}{1-\frac{2}{5}\left(0.5k_{m,p,n}\ell\right)^2}\frac{1}{j_{m,p}J_{m-1}\left(j_{m,p}\right)}\frac{k_{m,p,n}^2-\left(n\pi/h\right)^2}{k^2+kk_{m,p,n}\left(1+i\right)/Q_{m,p,n}^{\mathrm{cavity}}-k_{m,p,n}^2}\cos\left(\frac{n\pi z_{\mathrm{s}}}{h}\right) \tag{8}$$

with $k_{m,p,n} = \omega_{m,p,n}\sqrt{\mu_0\varepsilon_0} = \sqrt{\varsigma_{m,p}^2+\alpha_n^2}$, $\varsigma_{m,p,n} = \sqrt{k_{m,p,n}^2-\alpha_n^2}$, ε_0 the permittivity of free space, ϕ_{s} and z_{s} the physical location of the slot (note here $z_{\mathrm{s}} = 0$ is at the center of the cylinder), $Q_{m,p,n}^{\mathrm{cavity}} = \frac{\eta}{2R_S}\frac{\sqrt{\left(j_{m,p}\right)^2+\left(\alpha_n a\right)^2}}{1+\varepsilon_n a/h}$ is the cavity quality factor, $\eta = \sqrt{\mu_0/\varepsilon_0}$, and $\varepsilon_n = 1$ if $n = 0$, and $\varepsilon_n = 2$ if $n \neq 0$. The voltage drive $V\left(0\right)$ is proportional to the exterior short circuit current density at the center of the slot K_z^{sc}.

Figure Captions List

Fig. 1 (a) Schematic of a slotted cylindrical cavity excited by the marked plane-wave incident field. (b) Shielding effectiveness versus frequency around the TM_{010} mode assuming three values for the slot width *w*; other cavity parameters are kept as follows: *h* = 24 inch, *a* = 4 inch, $\sigma = 2.6 \times 10^7$ S/m , *d* = 0.25 inch, and $\ell_p = 2$ inch. An inset around the SE peak region is also shown.

Fig. 2 Main effects (first-order Sobol indices) S_j (solid lines) and total effects T_j (dotted lines) of shielding effectiveness versus slot and cavity parameters using the ranges reported in Table 1.

Fig. 3 Sensitivity analysis of shielding effectiveness versus slot and cavity parameters using the ranges reported in Table 1.

Fig. 4 Notional example of estimating the range of SE based on the ranges of uncertain inputs.

Fig. 5 Notional example of full uncertainty propagation of SE using probability distributions on the uncertain inputs.

Fig. 6 Interval uncertainty analysis for the unmatched formulation code (solid lines) and EIGER (dotted lines) for the SE peak of the TM010 mode supported by the cavity. The x-axis gives slot lengths; the slot width is represented with different colors; the slot depth is varied in left and right

panels. All the parameters considered here are listed in Table 2.

Fig. 7 Probability distributions of shielding effectiveness around the TM_{010} mode supported by the cavity assuming (a) normal or (b) uniform distribution for all the parameters considered in Table 1 and the down selected parameters shown in Table 2. The inset compares the normal and uniform cases for down selected parameters. All plots were generated using the distplot function in the Python package seaborn. Default settings for the histogram and kernel density estimate were used.

Table Caption List

Table 1 Uncertain inputs and their ranges used in sensitivity analysis.

Table 2 Slot length, width, and depth values for 4^3 full factorial design.

Table 3 Uniform and normal distributional assumptions for the probabilistic uncertainty analysis.

Table 4 Details of PCE construction for the four cases considered, including selected order and corresponding 10-fold cross-validation (CV) score.

Table 5 Mean, standard deviation, and select percentiles of peak TM_{010} shielding effectiveness.

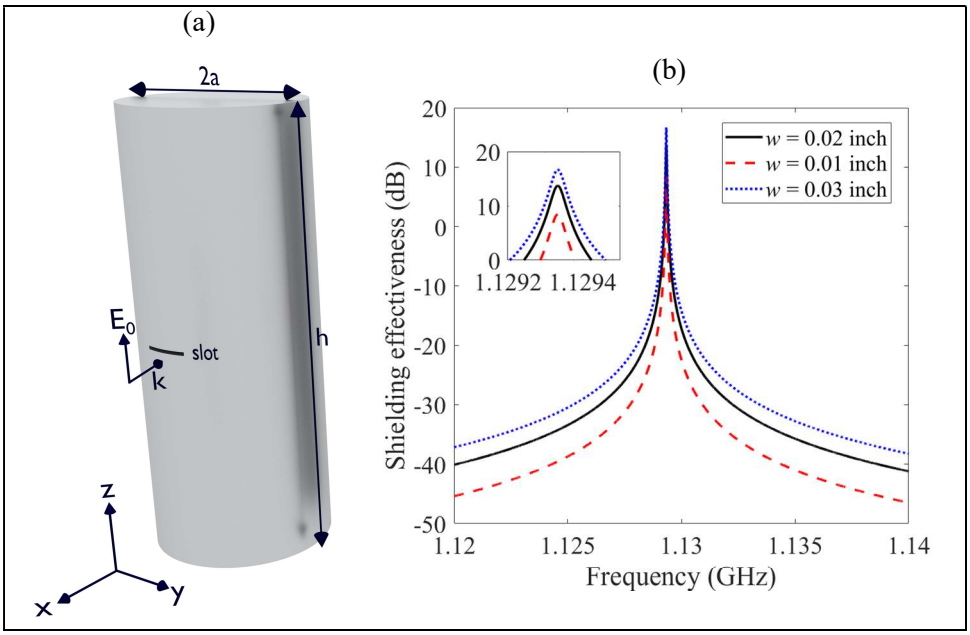

Fig. 1. (a) Schematic of a slotted cylindrical cavity excited by the marked plane-wave incident field. (b) Shielding effectiveness versus frequency around the TM_{010} mode assuming three values for the slot width *w*; other cavity parameters are kept as follows: *h* = 24 inch, *a* = 4 inch, $\sigma = 2.6 \times 10^7$ S/m , *d* = 0.25 inch, and $\ell_p = 2$ inch . An inset around the SE peak region is also shown.

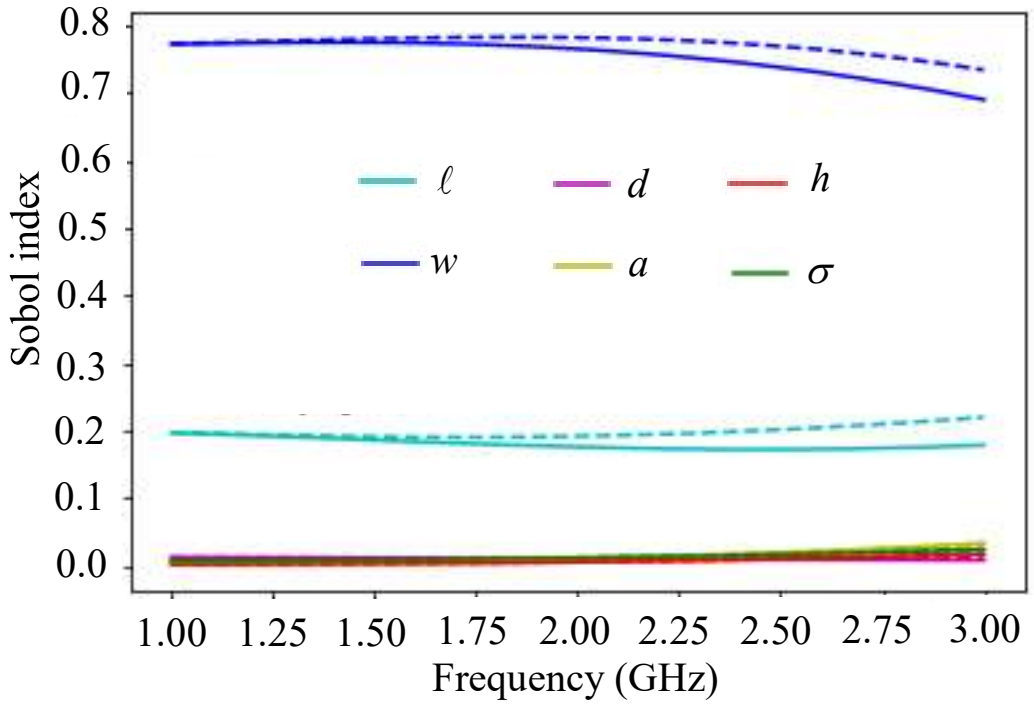

Fig. 2. Main effects (first-order Sobol indices) S_j (solid lines) and total effects T_j (dotted lines) of shielding effectiveness versus slot and cavity parameters using the ranges reported in Table 1.

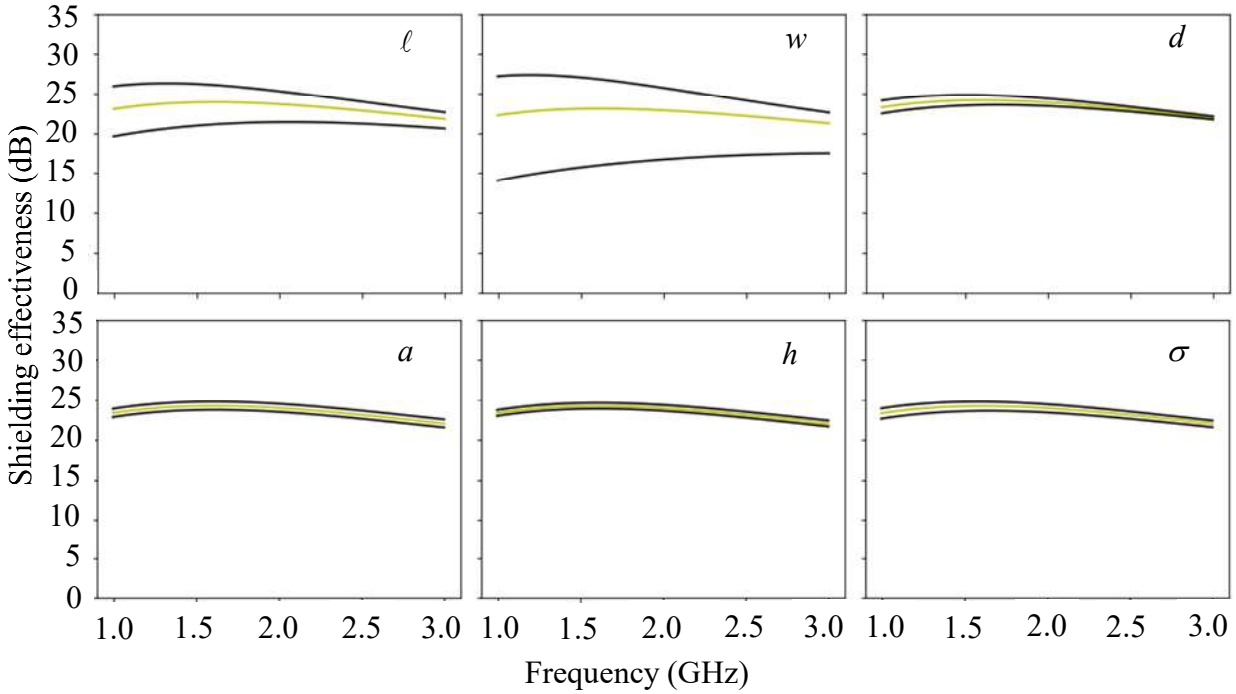

Fig. 3. Sensitivity analysis of shielding effectiveness versus slot and cavity parameters using the ranges reported in Table 1.

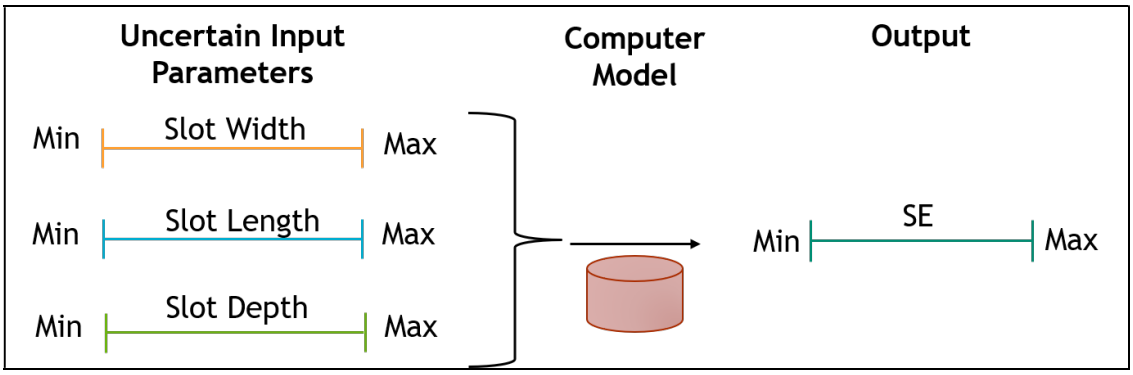

Fig. 4. Notional example of estimating the range of SE based on the ranges of uncertain inputs.

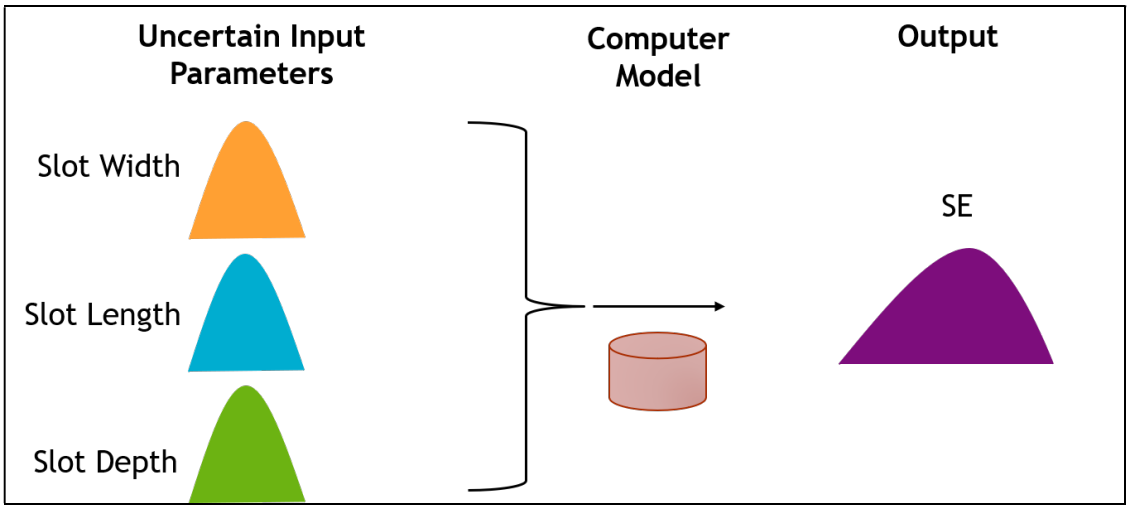

Fig. 5. Notional example of full uncertainty propagation of SE using probability distributions on the uncertain inputs.

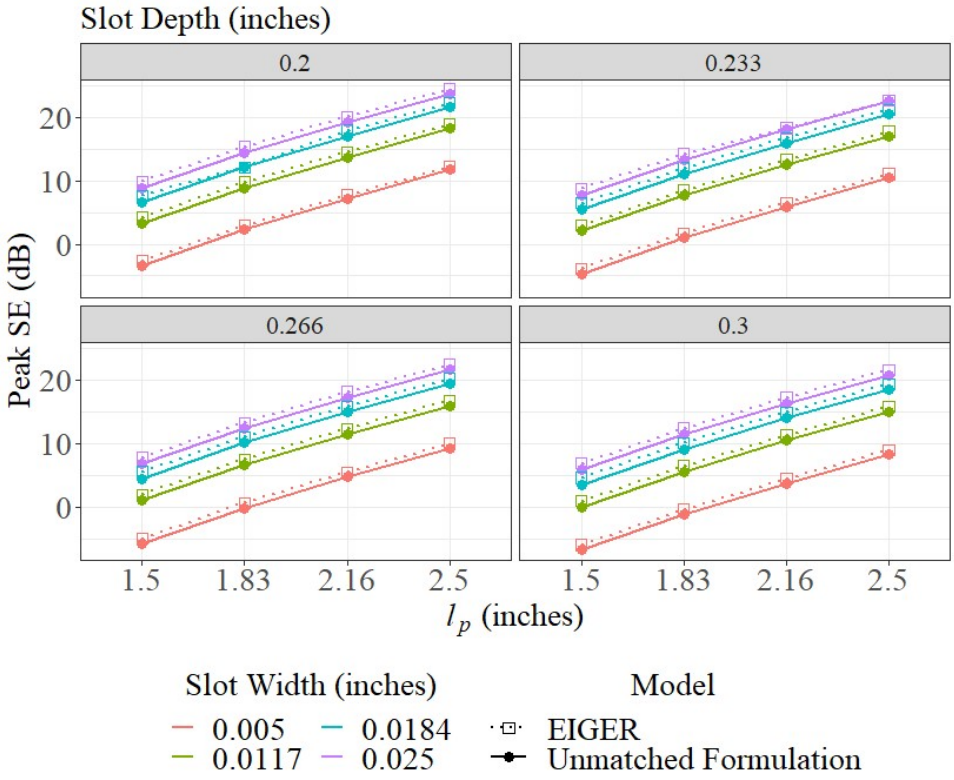

Fig. 6. Interval uncertainty analysis for the unmatched formulation code (solid lines) and EIGER (dotted lines) for the SE peak of the TM_{010} mode supported by the cavity. The x-axis gives slot lengths; the slot width is represented with different colors; the slot depth is varied in left and right panels. All the parameters considered here are listed in Table 2.

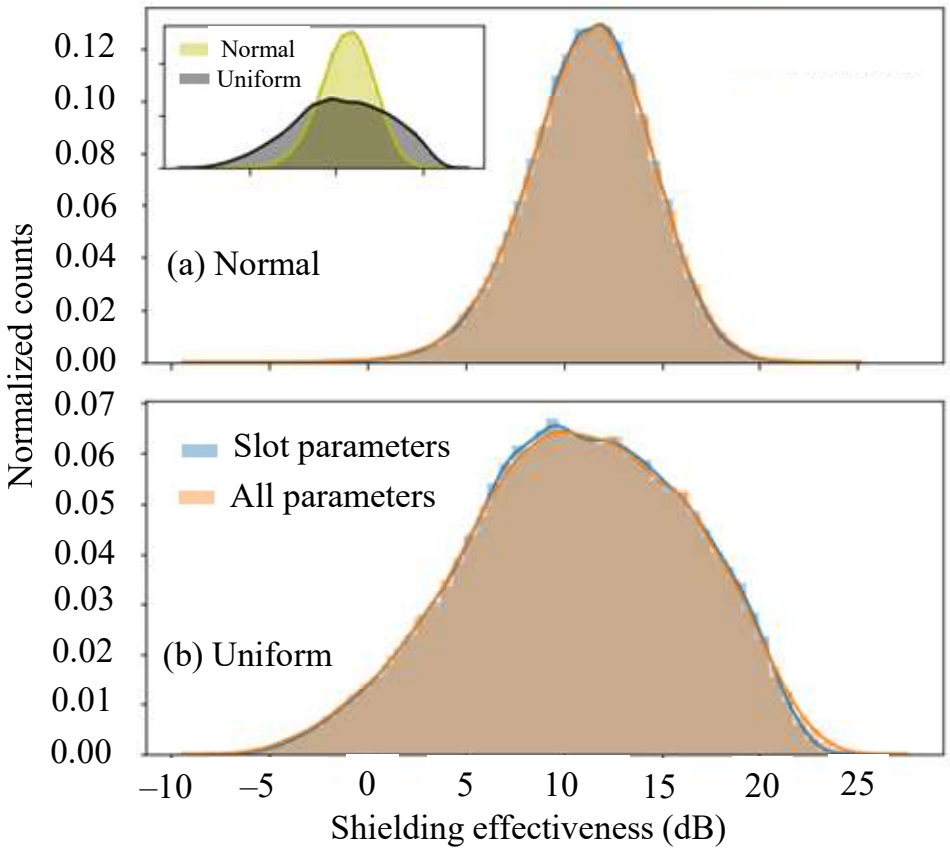

Fig. 7. Probability distributions of shielding effectiveness around the TM_{010} mode supported by the cavity assuming (a) normal or (b) uniform distribution for all the parameters considered in Table 1 and the down selected parameters shown in Table 2. The inset compares the normal and uniform cases for down selected parameters. All plots were generated using the distplot function in the Python package seaborn. Default settings for the histogram and kernel density estimate were used.

Table 1: Uncertain inputs and their ranges used in sensitivity analysis.

Input	***d* (in)**	ℓ_p **(in)**	***w* (mils)**	***h* (in)**	***a* (in)**	σ **(**$\times 10^7$ **S/m)**
Range	[0.2, 0.3]	[1.5, 2.5]	[5, 25]	[21.6, 26.4]	[3.6, 4.4]	[2.2, 3.0]

Table 2: Projected slot length, width, and depth values for 4^3 full factorial design.

Input	Level 1	Level 2	Level 3	Level 4
ℓ_p **(in)**	1.5	1.83	2.16	2.5
w **(mils)**	5	11.7	18.4	25
d **(in)**	0.2	0.233	0.266	0.3

Table 3: Uniform and normal distributional assumptions for the probabilistic uncertainty analysis.

Input		***d* (in)**	**ℓ (in)**	***w* (mils)**	***h* (in)**	***a* (in)**	**σ ($\times 10^7$ S/m)**
Normal	Mean	0.25	2.0	15.0	24.0	4.0	2.6
	Standard deviation	$0.01\overline{6}$	$0.1\overline{6}$	$3.\overline{3}$	0.8	$0.1\overline{3}$	$0.1\overline{3}$
Uniform	Lower bound	0.2	1.5	5.0	21.6	3.6	2.2
	Upper bound	0.3	2.5	25.0	26.4	4.4	3.0

Table 4: Details of PCE construction for the four cases considered, including selected order and corresponding 10-fold cross-validation (CV) score.

Distribution	Number of inputs	Selected order	CV score
Normal	6	4	3.57×10^{-3}
	3	5	6.06×10^{-5}
Uniform	6	5	2.46×10^{-4}
	3	5	1.07×10^{-4}

Table 5: Mean, standard deviation, and select percentiles of peak TM_{010} shielding effectiveness.

	Peak SE for normal inputs (dB)	**Peak SE for uniform inputs (dB)**
Mean	11.3	10.7
Standard deviation	3.1	5.5
5th percentile	6.0	1.2
25th percentile	9.3	6.8
50th percentile	11.4	10.8
75th percentile	13.4	14.9
95th percentile	16.1	19.4